ADAPTIVE SPACE-TIME FINITE ELEMENT METHODS FOR ACOUSTICS SIMULATIONS IN UNBOUNDED DOMAINS

PACS REFERENCE: 43.20.Px
Thompson, Lonny; He, Dantong
Clemson University, Department of Mechanical Engineering
Clemson, South Carolina 29634-0921 USA
(864)656-5631
email: lonny.thompson@ces.clemson.edu

ABSTRACT

High-order accurate and unconditionally stable time-discontinuous methods are implemented with nonreflecting boundary conditions in an adaptive space-time finite element method for acoustic radiation and scattering problems in exterior domains. An h-adaptive space-time procedure based on the Z^2 error estimate and the superconvergent patch recovery (SPR) technique, together with a temporal error estimate arising from the discontinuous jump in solution between time steps is used to maintain accuracy within a prescribed tolerance and drive dynamic mesh distributions. Error estimates of the nonreflecting boundaries are also monitored in the solution process. A new *superconvergent interpolation* method is developed for projection between adaptive meshes. Numerical studies of time-dependent scattering from an ellipse demonstrate the efficiency and reliability gained from the adaptive solution.

Introduction

We describe recent advances in the development of high-order accurate and unconditionally stable space-time methods which employ finite element discretization of the time domain as well as the usual discretization of the spatial domain. In particular, we examine the implementation of a sequence of high-order accurate radiation boundary conditions [1, 2, 3, 4] in an adaptive space-time finite element method for acoustic radiation and scattering problems in exterior domains. In particular, a multi-field discontinuous Galerkin finite element method (DGFEM) is used with independent acoustic pressure and velocity variables, [5, 6]. A multi-level iterative scheme is used to solve the resulting fully-discrete system equations for the interior hyperbolic equations coupled with the first-order temporal equations associated with auxiliary functions in the nonreflecting boundary conditions. The iterative strategy requires only a few iterations per time step to resolve the solution to high accuracy. An h-adaptive space-time strategy is employed based on the Zienkiewicz-Zhu [7] spatial error estimate using the superconvergent patch recovery (SPR) technique, together with a temporal error estimate arising from the discontinuous jump in velocity and pressure between time steps. As sound pulses propagate throughout the mesh, elements are refined near wave fronts, and unrefined where the solution is smooth or quiescent. Time-steps are also adjusted to maintain given error tolerances. Errors in the time integration of the auxiliary functions in the nonreflecting boundary conditions are also monitored and maintained within a tolerance. Numerical studies of transient scattering demonstrate the reliability and efficiency gained from the adaptive strategy.

Two-Dimensional Wave Equation on Unbounded Domains

We consider time-dependent waves in an infinite two-dimensional region $\mathcal{R} \subset \mathbb{R}^2$, surrounding an object with surface $\mathcal{S}$.

Within Ω, the solution $u(\boldsymbol{x}, t) : \Omega \times \mathbb{R}^+ \mapsto \mathbb{R}$, satisfies the scalar wave equation,

$$\frac{1}{c}\partial_t v \;=\; \nabla^2 u \;+\; f(\boldsymbol{x}, t), \qquad v = \frac{1}{c}\partial_t u, \qquad \boldsymbol{x} \in \Omega,\; t \in \mathbb{R}^+ \tag{1}$$

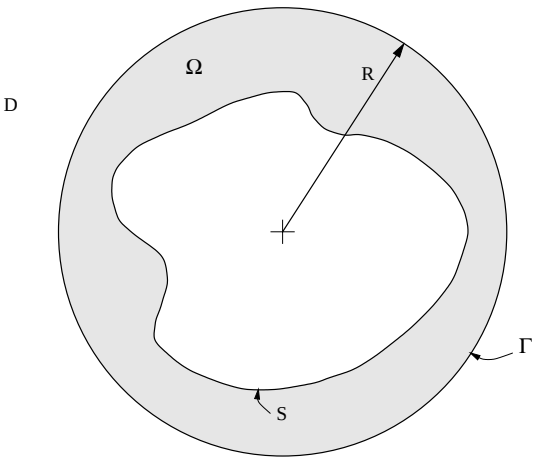

Figure 1: Illustration of two-dimensional unbounded region $\mathcal{R}$ surrounding a scatterer $\mathcal{S}$. The computational domain $\Omega \subset \mathcal{R}$ is surrounded by a circular truncation boundary Γ of radius R, with exterior region $\mathcal{D} = \mathcal{R} - \Omega$.

with initial conditions, $u(\boldsymbol{x}, 0) = u_0(\boldsymbol{x}), v(\boldsymbol{x}, 0) = v_0(\boldsymbol{x})$. On the scatterer, we can specify a Neumann boundary condition, $\partial_n u = g(\boldsymbol{x}, t)$, $\boldsymbol{x} \in \mathcal{S},\ t \in \mathbb{R}^+$.

We denote the solution evaluated on the circular truncation boundary at $r = R$ by,

$$u_\Gamma(\theta, t) = u(R, \theta, t), \qquad v_\Gamma(\theta, t) = \frac{1}{c}\partial_t u_\Gamma, \qquad \theta \in [0, 2\pi),\ t \in \mathbb{R}^+, \tag{2}$$

Let $\boldsymbol{w}(\theta, t) = \{w_j(\theta, t)\}_{j=1}^p$, be defined as a time-dependent vector of real valued scalar auxiliary functions, i.e., $\boldsymbol{w} = (w_1\,, w_2\,, \cdots, w_p)$. We can expand the auxiliary functions $\boldsymbol{w}(\theta, t)$ and solution on the truncation boundary $u_\Gamma(\theta, t)$ by a Fourier series,

$$u_\Gamma(\theta, t) = \sum_{m=-\infty}^{\infty} u_m(t)\ \mathrm{e}^{im\theta}, \qquad \boldsymbol{w}(\theta, t) = \sum_{m=-M}^{M} \boldsymbol{w}_m(t)\ \mathrm{e}^{im\theta} \tag{3}$$

with complex-valued Fourier modes $u_m(t) : \mathbb{R}^+ \mapsto \mathbb{C}$, and $\boldsymbol{w}_m(t) = \{w_m^j\}_{j=1}^p$, $w_{m,j}(t) : \mathbb{R}^+ \mapsto \mathbb{C}$, defined by the tangential Fourier transform:

$$u_m(t) = \frac{1}{2\pi}\int_0^{2\pi} u_\Gamma(\theta, t)\ \mathrm{e}^{-im\theta}\, d\theta, \qquad \boldsymbol{w}_m(t) = \frac{1}{2\pi}\int_0^{2\pi} \boldsymbol{w}(\theta, t)\ \mathrm{e}^{-im\theta}\, d\theta. \tag{4}$$

Here $u_m = u_{-m}^*$, and $\boldsymbol{w}_m = \boldsymbol{w}_{-m}^*$, with the asterisk denoting the complex conjugate, and $i = \sqrt{-1}$.

Using this expansion, we then approximate the exterior impedance on Γ, by the sequence of high-order accurate radiation boundary conditions derived in [4]:

$$\partial_r u|_{r=R} + v_\Gamma(\theta, t) + \frac{1}{2R}u_\Gamma(\theta, t) = \sum_{m=-N}^{N} w_m^1(t)\,\mathrm{e}^{im\theta} \tag{5}$$

$$\boldsymbol{w}_m'(t) + \boldsymbol{A}_m\,\boldsymbol{w}_m(t) = \boldsymbol{b}_m\,u_m(t), \qquad \boldsymbol{w}_m(0) = 0 \tag{6}$$

In the above, the prime indicates a derivative; $\boldsymbol{w}_m(t)$ are time-dependent vector functions of order p, and $\boldsymbol{A}_m = \{A_m^{ij}\}_{i,j=1}^p$, is a tri-diagonal matrix for each mode m, see [4]. The constant vector $\boldsymbol{b}_m = \{b_m^j\}_{j=1}^p$ is defined by $\boldsymbol{b}_m = \frac{c}{8R^2}(1 - 4m^2)\,\boldsymbol{e}_1$.

Discontinuous Galerkin FEM

The development of the space-time method proceeds by considering a partition $\mathcal{M}$ of the total time interval, $t \in J = (0, T), 0 < T < \infty$, into N time steps $\{I_n\}_{n=0}^N$ given by $I_n = \{(t_n, t_{n+1})\}_{n=0}^N$. The length of the variable time step is given by $\Delta t_n = t_{n+1} - t_n$. Using this notation, $Q_n = \Omega \times I_n$, are the nth space-time slabs. Within each space-time slab, the spatial domain is subdivided into D_n elements. We define the jump operator across space-time slabs as,

$$[\![u(t_n)]\!] \,=\, u(\boldsymbol{x}\,, t_n^+) \,-\, u(\boldsymbol{x}\,, t_n^-), \quad 0 \le n \le N$$

Standard L_2 inner products are denoted, $(w\,, u) = \int_\Omega w\,u\,d\boldsymbol{x}$, equipped with norm $||u||_\Omega = (u\,, u)^{1/2}$. Integrals on boundaries are defined by, $(w\,, u)_\Gamma = \frac{1}{2R}\int_\Gamma w\,u\,d\Gamma$, $(w\,, u)_S = \int_S w\,u\,dS$.

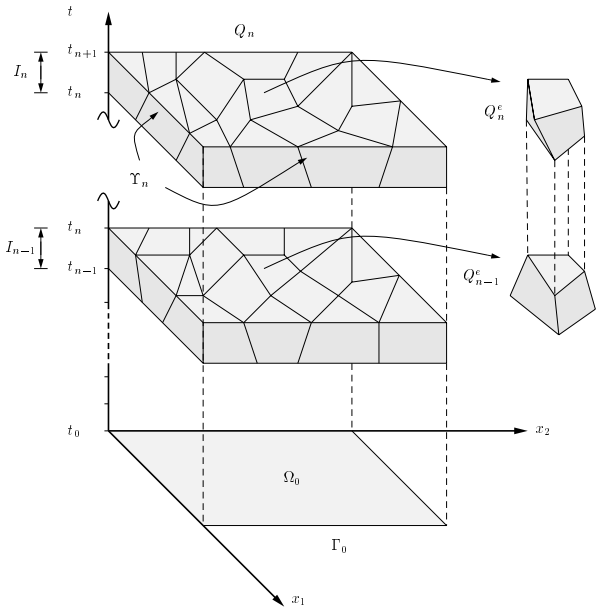

Figure 2: Illustration of two consecutive space-time slabs Q_{n-1} and Q_n, each with different meshes. Within each space-time element, the trial solution and weighting function are approximated by a finite basis which depend on both spatial $\boldsymbol{x}$, and temporal t, dimensions. The basis functions are assumed $C^0(Q_n)$ continuous throughout each space-time slab, but are allowed to be discontinuous across the interfaces of the slabs. The space of finite element basis functions in our multi-field representation is stated in terms of *independent* variables u, and v.

The statement of the time-discontinuous Galerkin method may be stated as
Given: Load data f , g, and initial conditions $\{u(\boldsymbol{x},t_n^-), v(\boldsymbol{x},t_n^-)\}$, $\boldsymbol{w}_m(t_n^-)$, from the previous time step, then for each space-time slab, $n = 0, 1, \ldots, N-1$; *Find:* $\boldsymbol{u} = \{u(\boldsymbol{x},t), v(\boldsymbol{x},t)\}$, and $\boldsymbol{w}_m(t)$, $\boldsymbol{x} \in \Omega \cup \partial\Omega$, $t \in I_n = (t_n, t_{n+1})$, such that for all admissible functions $\bar{\boldsymbol{u}} = \{\bar{u}(\boldsymbol{x},t), \bar{v}(\boldsymbol{x},t)\}$, and $\bar{\boldsymbol{w}}_m(t)$, $m \in (-M, M)$, the following coupled integral equations are satisfied,

$$A(\bar{\boldsymbol{u}}\,,\,\boldsymbol{u})_n + B_\Gamma(\bar{\boldsymbol{u}}\,,\,\boldsymbol{u})_n = F_S(\bar{v})_n + F_\Gamma(\bar{v}, w_m^1) \tag{7}$$

$$A_m(\bar{\boldsymbol{w}}_m\,,\,\boldsymbol{w}_m)_n = F_m(\bar{w}_m^1, u_m), \quad m \in (-M, M) \tag{8}$$

with

$$\begin{aligned} A(\bar{\boldsymbol{u}}\,,\,\boldsymbol{u})_n &:= \int_{I_n} \left\{ (\bar{v}\,,\,\partial_t v) + (\nabla\bar{v}\,,\,\nabla u) + (\nabla\bar{u}\,,\,\frac{1}{c}\nabla\partial_t u - \nabla v) \right\} \,\mathrm{d}t \\ &\quad + (\bar{v}(t_n^+)\,,\,[\![v(t_n)]\!]) + (\nabla\bar{u}(t_n^+)\,,\,[\![\nabla u(t_n)]\!]) \\ B_\Gamma(\bar{\boldsymbol{u}}\,,\,\boldsymbol{u})_n &:= \int_{I_n} \left\{ 2R(\bar{v}\,,\,v)_\Gamma + (\bar{v}\,,\,u)_\Gamma + (\bar{u}\,,\,\frac{1}{c}\partial_t u - v)_\Gamma \right\} \,\mathrm{d}t + (\bar{u}(t_n^+)\,,\,[\![u(t_n)]\!])_\Gamma \end{aligned}$$

$$\begin{aligned} A_m(\bar{\boldsymbol{w}}_m\,,\,\boldsymbol{w}_m)_n &:= \int_{I_n} \{\bar{\boldsymbol{w}}_m(t)\cdot\boldsymbol{w}_m'(t) + \bar{\boldsymbol{w}}_m(t)\cdot\boldsymbol{A}_m\,\boldsymbol{w}_m(t)\} \,\mathrm{d}t + \bar{\boldsymbol{w}}_m(t_n^+)\cdot[\![\boldsymbol{w}_m(t_n)]\!] \\ F_m(\bar{w}_m^1, u_m) &:= b_m^1 \int_{I_n} \bar{w}_m^1(t)\,u_m(t)\,\mathrm{d}t \\ F_\Gamma(\bar{v}, w_m^1) &:= 2R\sum_{m=-M}^{M} \int_{I_n} (\bar{v}\,,\,\mathrm{e}^{im\theta})_\Gamma\, w_m^1(t)\,\mathrm{d}t \end{aligned}$$

On a typical current time slab $I_n = (t_n, t_{n+1}) = (t_1, t_2)$, with length $\Delta t_n = t_2 - t_1 > 0$, and temporal approximation order r, the DGFEM is found by solving the coupled variational problem (7)-(8). The source $f(\boldsymbol{x},t)$, Neumann data $g(\boldsymbol{x},t)$, initial conditions from the previous time-step $\{u(\boldsymbol{x},t_n^-), v(\boldsymbol{x},t_n^-)\}$, and $\boldsymbol{w}_m(t_n^-)$, are the known data on the time slab. Coupling occurs through drivers $\boldsymbol{w}_m(t)$ on the right-hand-side of Eq. (7), and boundary modes $u_m(t)$, defined by (4) on the right-hand-side of (8).

Space-Time Discretization of the Hyperbolic Wave Equation

In this paper, within a space-time slab, $Q_n = \Omega \times I_n$, we assume an orthogonal space-time discretization with linear temporal approximation,

$$u(\boldsymbol{x},t) = \sum_{i=1}^{2} u_i^h(\boldsymbol{x})\phi_i(t) = \boldsymbol{N}_n(\boldsymbol{x})\sum_{i=1}^{2}\phi_i(t)\boldsymbol{d}_i \tag{9}$$

where $\{\phi_i\}_{i=1}^2$ are basis functions of $\mathcal{P}^1(I_n)$. These basis functions may be high-order spectral, defined by continuous Lagrange interpolation, or p-version, defined by hierarchical Legendre polynomials. The FE approximations of $\{u_i\}$ are given as linear combinations of basis functions N_A, and $\boldsymbol{d}_i = \{u_A(t_i)\}_{A=1}^{D_n}$. The solution at the bottom is denoted, $t_1 = t_n^+$, and top, $t_2 = t_{n+1}^-$, the initial condition from the previous step is denoted $t_0 = t_n^- = t_{n-1}^+$. Similarly, $v(\boldsymbol{x},t) = \sum_{i=1}^2 v_i^h(\boldsymbol{x})\phi_i(t) = \boldsymbol{N}_n(\boldsymbol{x})\sum_{i=1}^2 \phi_i(t)\boldsymbol{c}_i$. The time-dependent auxiliary functions approximated by,

$$\boldsymbol{w}_m(t) = \sum_{i=1}^{2} \boldsymbol{w}_{m,i}\phi_i(t) \tag{10}$$

Substituting the space-time approximations into the space-time variational equations results in the fully discrete matrix problem,

$$\begin{bmatrix} \hat{\boldsymbol{M}} & \hat{\boldsymbol{M}}_{12} \\ \hat{\boldsymbol{M}}_{21} & \hat{\boldsymbol{M}} \end{bmatrix} \begin{Bmatrix} \boldsymbol{c}_1 \\ \boldsymbol{c}_2 \end{Bmatrix} = \begin{Bmatrix} \hat{\boldsymbol{r}}_1 \\ \hat{\boldsymbol{r}}_2 \end{Bmatrix} \tag{11}$$

where $\hat{\boldsymbol{M}} = \boldsymbol{M} + \frac{\Delta t}{4}\boldsymbol{C}$. $\hat{\boldsymbol{M}}_{12}$ and $\hat{\boldsymbol{M}}_{21}$ depend on the the mass,damping,and stiffness matrices $\boldsymbol{M},\boldsymbol{C},\boldsymbol{K}$. The rhs vectors are functions of: $\hat{\boldsymbol{r}}_i = \boldsymbol{r}_i(\boldsymbol{f}_i,\boldsymbol{c}_0,\boldsymbol{M},\boldsymbol{K},\Delta t)$, The displacements are simply updated with,

$$\boldsymbol{d}_1 = \boldsymbol{d}_0 + \frac{\Delta t}{6}(\boldsymbol{c}_1 - \boldsymbol{c}_2), \qquad \boldsymbol{d}_2 = \boldsymbol{d}_0 + \frac{\Delta t}{2}(\boldsymbol{c}_1 + \boldsymbol{c}_2) \tag{12}$$

$\boldsymbol{d}_0 = \boldsymbol{d}(t_n^-)$, and $\boldsymbol{c}_0 = \boldsymbol{c}(t_n^-)$ are initial conditions from the previous time-step. The load vectors do to the coupling from the auxiliary function $w_m^1(t)$ are given by,

$$\boldsymbol{f}_j^\Gamma = 2R\sum_{m=-M}^{M} w_{m,j}^1 \boldsymbol{F}_m, \quad \boldsymbol{F}_m = \{F_A^m\}, \quad F_A^m := (N_A, e^{im\theta})_\Gamma$$

The time discretization for the first-order boundary equations takes the form,

$$\begin{bmatrix} \boldsymbol{I} & -(\boldsymbol{I} + \frac{\Delta t}{3}\boldsymbol{A}_m) \\ 3(-\boldsymbol{I} + \frac{\Delta t}{3}\boldsymbol{A}_m) & \boldsymbol{I} \end{bmatrix} \begin{Bmatrix} \boldsymbol{w}_{m,1} \\ \boldsymbol{w}_{m,2} \end{Bmatrix} = \begin{Bmatrix} \hat{\boldsymbol{f}}_{m,1} \\ \hat{\boldsymbol{f}}_{m,2} \end{Bmatrix} \tag{13}$$

where the rhs vectors are driven by $\boldsymbol{w}_m(t_n^-)$, and the modes $u_{m,j}$,

$$u_m(t) = \sum_{i=1}^{2} u_{m,j}\phi_i(t), \quad u_{m,j} = \frac{1}{\pi}\boldsymbol{F}_{m,n}^* \cdot \boldsymbol{d}_j \tag{14}$$

A remarkable feature of this form is that for spectral interpolation in space, nodal quadrature may be used to diagonalize both $\boldsymbol{M}$ and $\boldsymbol{C}$, resulting a diagonal mass matrix and complete decoupling of the equations of the upper and lower sub-block diagonals. In this case, each time step requires only matrix-vector products with $\hat{\boldsymbol{M}}_{12}$ at each iteration in the solution for $\boldsymbol{c}_1$ and $\boldsymbol{c}_2$. Wiberg and Lee [8] derived a different form, with $\hat{\boldsymbol{M}} = \boldsymbol{M} + \frac{\Delta t}{2}\boldsymbol{C} + \frac{\Delta t}{6}\boldsymbol{K}$; this submatrix cannot be convieniently diagonalized because of the presence of $\boldsymbol{K}$.

The order p used in the radiation boundary is typically less than $p < 10$, resulting in relatively small matrices $\boldsymbol{A}_m$. The number of modes $m \in (-M, M)$ included depends on the complexity of the solution as measured by the amplitude of spatial angular wavelengths on the boundary Γ; typically $M \ll N_\Gamma$, where N_Γ is the number of nodes on the boundary. The primary cost in implementing the high-order radiation boundary conditions is not the solution of the equation system (13), but in the computation of the discrete Fourier transform $u_{m,j}$, which must re-evaluated at each adaptive remeshing. Nevertheless, this cost is always less that that required to solve the interior equations for $(\boldsymbol{d}_j, \boldsymbol{c}_j)$; see [4]. A multi-level iterative method is used between (11) and (13); system (11) is solved with a simple Gauss-Seidel iterative algorithm, while the relatively small system (13) is solved directly. Using the initial predictor from the previous time-step, only a few iterations are needed to solve the coupled equations.

Projection of the solution from the previous space-time slab to the current space-time slab is obtained by nodal interpolation. For low-order elements in space, standard nodal interpolation introduces significant error. To correct this difficulty, we have developed a new *superconvergent*

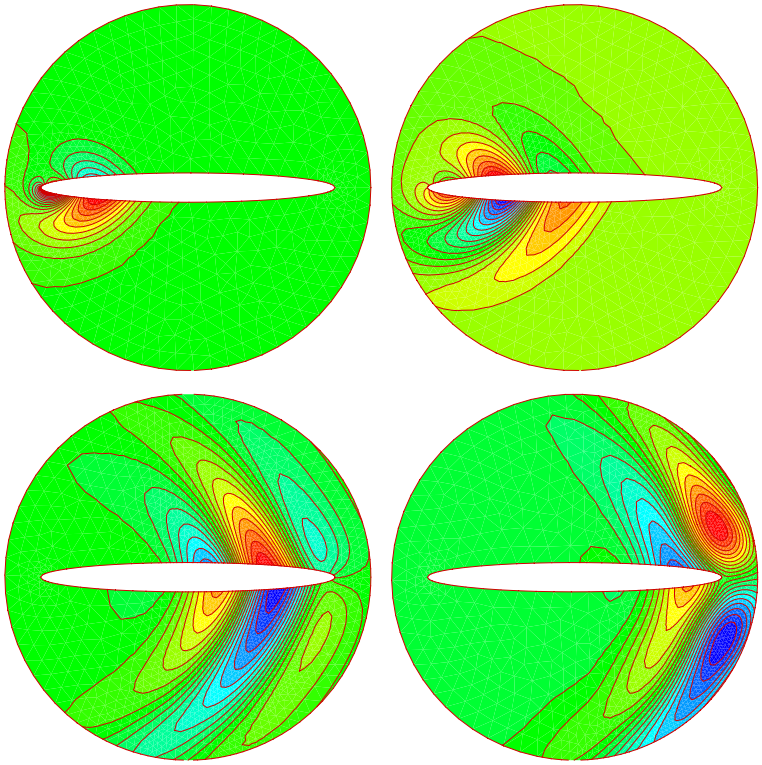

Figure 1: Scattered field solution at snapshots in time.

interpolation scheme. Prior to projecting, the solution on the top of previous time-slab, t_n^-, is interpolated with,

$$u(\boldsymbol{x}, t_n^-) = \sum_{A=1}^{D_{n-1}} N_A^-(\boldsymbol{x}) \left[u_A^h(t_n^-) + \Delta \boldsymbol{x}_A \cdot \nabla u_A^*(\boldsymbol{x}_A^c, t_n^-) \right] \tag{15}$$

where, $\Delta \boldsymbol{x}_A = (\boldsymbol{x} - \boldsymbol{x}_A)$ and the vector, $\nabla u_A^*(\boldsymbol{x}_A^c, t_n^-)$ is the recovered gradients obtained by superconvergent patch recovery (SPR) at node A, [7] evaluated at the midpoint between node $\boldsymbol{x}_A$, and position $\boldsymbol{x}$. A similar technique is used for $v(\boldsymbol{x}, t_n^-)$. This scheme may be viewed as a correction to standard interpolation, and provides nearly an order-of-magnitude improvement in accuracy. The spatial and temporal error estimates and adaptive strategy we use is similar to that given in [8]; the main improvements are the use of our superconvergent interpolation (projection) technique together with an improved mesh distribution parameter [9].

Numerical Example

Consider scattering of a plane wave at 30^o incidence, defined by a Ricker pulse, by a rigid elliptic cylinder. The high-order $p = 6$, nonreflecting boundary conditions are applied on a surrounding circle. Figure 1 shows the adaptive solution on linear triangles with spatial, and temporal error tolerances 10% and 0.5% respectively. The corresponding spatial mesh tracking the scattered solution is shown in Figure 2.

Conclusions

Comprehensive adaptive procedures for DGFEM including high-order accurate nonreflecting boundary conditions for unbounded problems has been developed. Computationally efficient matrix structures are used together with a multi-level iterative solver strategy for efficient and accurate solutions to the wave equation coupled with nonreflecting boundaries. The iterative strategy requires only a few iterations per time step to resolve the solution to high accuracy. Error estimators are computed to maintain accuracy within a prescribed tolerance and used to drive optimally distributed meshes and time-steps. A new superconvergent interpolation is developed for accurate projection between space-time stabs in the adaptive process.

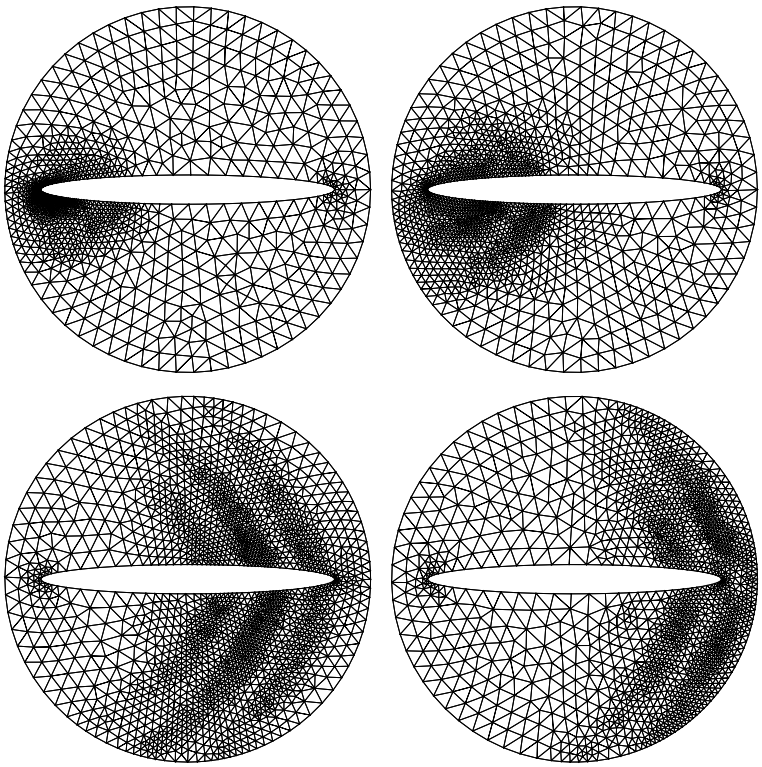

Figure 2: Adaptive mesh tracking scattered solution.

Support for this work was provided by the National Science Foundation under Grant CMS-9702082 in conjunction with a Presidential Early Career Award for Scientists and Engineers (PECASE).

References

[1] Thompson, L.L., and Huan, R., "Computation of Far Field Solutions Based on Exact Nonreflecting Boundary Conditions for the Time-Dependent Wave Equation", *Computer Methods in Applied Mechanics and Engineering*, 190, (2000), 1551-1577.

[2] Thompson, L.L., and Huan, R., "Computation of Transient Radiation in Semi-Infinite Regions Based on Exact Nonreflecting Boundary Conditions and Mixed Time Integration", *Journal of the Acoustical Society of America*, 106 (6), pp. 3095-3108, December 1999.

[3] Huan, R., and Thompson, L.L., 'Accurate Radiation Boundary Conditions for the Time-Dependent Wave Equation on Unbounded Domains', *International Journal for Numerical Methods in Engineering*, 47, pp. 1569 - 1603, 2000.

[4] Thompson, L.L., and Huan, R., D. He; "Accurate radiation boundary conditions for the two-dimensional wave equation on unbounded domains", *Computer Methods in Applied Mechanics and Engineering*, 191 (2001) 311-351.

[5] Thompson, L.L., and Pinsky, P.M., "A Space-time finite element method for the exterior structural acoustics problem: Time-dependent radiation boundary conditions in two spatial dimensions", *International Journal for Numerical Methods in Engineering*, **39**, pp. 1635-1657, 1996.

[6] Thompson, L.L., "A multi-field space-time finite element method for structural acoustics", *Proceedings of the 1995 Design Engineering Technical Conferences*, *Acoustics, Vibrations, and Rotating Machines*, Vol. 3, Part B, ASME, pp. 49 - 64, Boston, Mass., Sept. 17-21, 1995.

[7] O. C. Zienkiewicz, J. Z. Zhu, 'The superconvergent patch recovery and a posterior error estimates. Part 1: The Recovery technique', *International Journal for Numerical Methods in Engineering*, Vol.**33**, 1331-1364, 1992.

[8] Li, X., Wiberg, N.-E., 'Implementation and adaptivity of a space-time finite element method for structural dynamics', *Computational Methods in Applied Mechanics and Engineering*, **156**, 211-229, 1998.

[9] P. Coorevits, P. Ladeveze, J.-P. Pelle, 'An automatic procedure with a control of accuracy for finite element analysis in 2D elasticity', *Computational Methods in Applied Mechanics and Engineering*, **121**, 91-120, 1995.